Available online at www.sciencedirect.com
ScienceDirect
Journal of Crystal Growth 310 (2008) 2264–2267
JOURNAL OF CRYSTAL GROWTH
www.elsevier.com/locate/jcrysgro

Tunable light emissions from thermally evaporated In_2O_3 nanostructures grown at different growth temperatures

Tsung-Shine Ko, Chia-Pu Chu, Jun-Rong Chen, Tien-Chang Lu*, Hao-Chung Kuo*, Shing-Chung Wang

Department of Photonics and Institute of Electro-Optical Engineering, National Chiao Tung University, 1001 Ta Hsueh Rd., Hsinchu 30050, Taiwan, ROC

Available online 4 December 2007

Abstract

We report the synthesis of the In_2O_3 nanostructures grown at different growth temperatures by using the thermal evaporation method. The gold nanoparticles were used as the catalyst and were dispersed on the silicon wafer to facilitate the growth of In_2O_3 nanostructures. The nanostructures of the In_2O_3 were characterized by scanning electron microscopy, transmission electron microscopy, and X-ray diffraction. The photoluminescence study reveals that In_2O_3 nanostructures could emit different luminescence peaks in the range of 400–600 nm with broad bands by adjusting different growth temperatures. The coverage of the wavelength tuning in the emission peaks of the In_2O_3 nanostructures could be beneficial for possible applications in white light illumination through manipulating the ratio of each wavelength component.

PACS: 81.10.−h; 81.10.BK; 42.70.−a

Keywords: A1. Nanostructure; A1. Photoluminescence; B1. Indium oxide; B2. Semiconducting indium compound

1. Introduction

In_2O_3 is an important transparent semiconductor material with wide band gap energy (3.6 eV) and has been applied in optical and electric devices such as solar cells and liquid crystal devices [1–3]. Previous studies focused on the preparations and characterizations of In_2O_3 films or nanostructrues [4,5]. However, optical properties, such as photoluminescence (PL) results of In_2O_3 obtained by different research groups varied a lot. For instance, Lee et al. obtained the PL emission of 637 nm from In_2O_3 thin films synthesized by thermal oxidation [4]. Liang et al. used InP as the starting material to grow In_2O_3 nanofibers using a furnace and their PL spectra exhibited emission of 470 nm [6]. Zheng et al. observed the PL emission of 429 and 460 nm from their In_2O_3 nanowires using a three-probe DC method [7]. Li et al. measured PL of In_2O_3 nanotubes exhibiting emission of 593 nm [8]. Most of the above PL results come from different densities of oxygen vacancies [9]. However, few groups have developed methods to modulate the emission wavelength of In_2O_3. In this paper, we report the synthesis of In_2O_3 nanoparticles with a special nanostructure using the two-zone thermal evaporation method. The PL results of In_2O_3 nanostructures obtained by different growth conditions exhibited different broad band emission peaks ranging from 400 to 600 nm, which could have potential applications in white light illumination.

2. Experiments

The synthesis procedures of In_2O_3 nanostructures started with gold nanoparticles produced by the chemical reduction of gold chloride tetrahydrate ($HAuCl_4$) with sodium citrate spread onto the Si substrates cleaned by the 3-aminopropyl-trimethoxysilan (APTMS) ethanol solution and water. Observed from the SEM (scanning electron microscopy) images, the Au nanoparticles are 10–20 nm in width and the density is around $6 \times 10^8\,cm^{-2}$. Then, the gold nanoparticles

*Corresponding authors. Tel.: +886 3 5712121x52962; fax: +886 3 5716631.
E-mail addresses: timtclu@faculty.nctu.edu.tw (T.-C. Lu), hckuo@faculty.nctu.edu.tw (H.-C. Kuo).

0022-0248/$ - see front matter © 2007 Elsevier B.V. All rights reserved.
doi:10.1016/j.jcrysgro.2007.11.173

on Si substrates were sent to a two-zone vacuum furnace to grow the In_2O_3. The experimental setup for synthesizing indium oxide nanostructures is schematically depicted in Fig. 1. The starting material, 5 g indium metal, was placed in a quartz boat located inside a quartz tube reactor, designated as zone 1 with the temperature setting as $T1$. p-Type silicon (1 0 0) substrates were placed in the downstream of the tube reactor separated from the starting material by 20 cm, designated as zone 2 with the temperature setting as $T2$. The quartz tube was exhausted by a mechanical pump down to around 0.1 Torr. We grew indium oxide nanostructures under different growth temperatures $T2$ from 500 to 900 °C for 8 h reaction time. The temperature $T1$ was set 900 °C for the source zone. We used the oxygen gas of 150 sccm as carrier gas in our furnace system.

For characterization of as-grown samples, we used SEM (JEOL, JSM 6500F) and high-resolution transmission electron microscopy (HRTEM, JEOL, JEM 2010F, operating at 200 kV) to investigate the morphology and microstructure. The compositions were analyzed using energy dispersive spectrometry (EDS) attached to the SEM. Selected area electronic diffraction (SAED) confirmed the crystal orientation of In_2O_3 nanocrystals. The crystal structure analysis was performed by the XRD measurement with Cu Kα radiation. PL spectra were measured at room temperature with a spectrometer (TRIAX-320) excited by a 25-mW He–Cd laser with the lasing wavelength of 325 nm.

3. Results and discussion

Fig. 2(a)–(c) show SEM images of the In_2O_3 nanocrystals grown at different growth temperatures of 500, 700, and 900 °C, respectively, with the oxygen flow rate of 150 sccm. The amount of nanostructure was found to be dependent on the growth temperatures. As a result, Fig. 2(a) shows fewer nanostructures existed and many In_2O_3 tips are beginning to sprout when the growth temperature was 500 °C. As the growth temperature was increased to 900 °C, most of In_2O_3 nanocrystals show well-shaped nanostructure as indicated in Fig. 2(c).

The HRTEM images of the nanostructure grown with the oxygen flow rate of 150 sccm at 700 °C are shown in Fig. 3(a) and (b). It is clearly shown that the In_2O_3 nanostructure was capped with a 20-nm gold nanoparticle. The presence of gold nanoparticles at the top of the In_2O_3 nanostructures provides a strong evidence of the vapor–liquid–solid (VLS) growth mechanism. However, VLS growth mechanism generally leads to a well-directional growth and further to form nanowire or nanorod structures [10,11], which is different from our results. We proposed that the short In_2O_3 nanowires were nucleated at the gold nanoparticles by the VLS mechanism at first. As the growth time passed by, the growth direction still favored to the top due to the fast reaction provided by the catalyst. However, the over-supply of the indium vapor

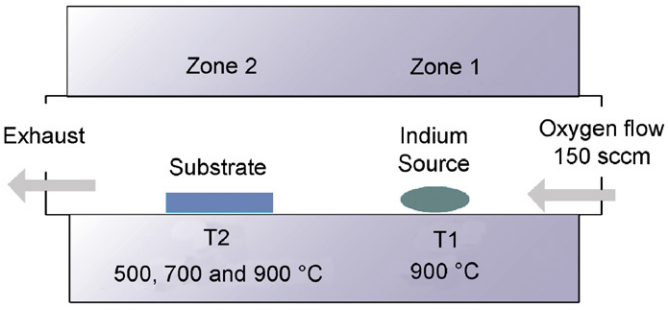

Fig. 1. Schematic diagram of a two-zone furnace for indium oxide nanostructures' growth.

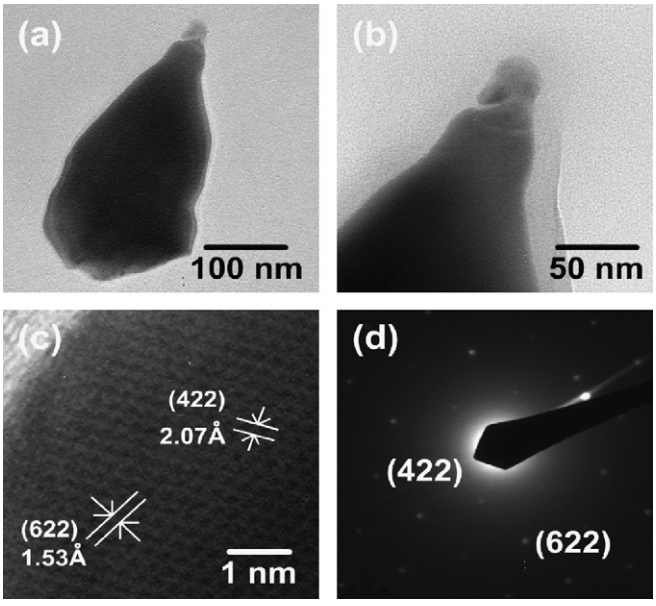

Fig. 3. (a, b) TEM images of the In_2O_3 nanostructure's tip. (c) High-resolution TEM images of part of the In_2O_3 nanostructures. (d) The corresponding selected area electron diffraction pattern. This In_2O_3 nanostructure was grown at 700 °C.

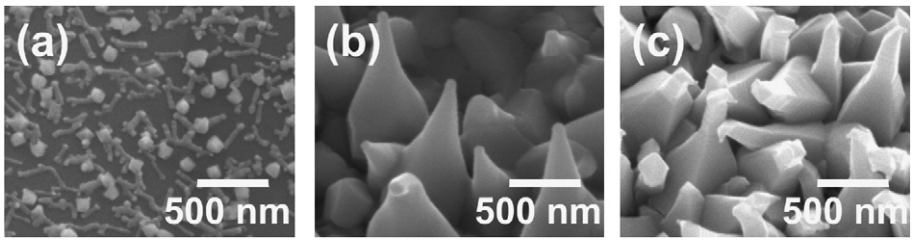

Fig. 2. In_2O_3 nanostructures grown at different growth temperatures of 500, 700, and 900 °C (a)–(c), respectively.

interacting with oxygen atoms could further facilitate the lateral growth. The lateral volume could increase and then turned into such a special shape. Fig. 3(c) and (d) show HRTEM image of a partial In_2O_3 nanostructure and the corresponding SAED result, which proved that our In_2O_3 nanostructure was a single crystal structure. The lattice plane of (4 2 2) with an interplanar spacing of 0.207 nm and (6 2 2) with spacing of 0.153 nm can be obtained by the analysis of both TEM images and SAED shown in Fig. 3 corresponding to the In_2O_3 crystal lattice planes.

Typical XRD patterns of the In_2O_3 nanostructures grown at different growth temperatures are shown in Fig. 4. All the diffraction peaks could be indexed to a pure cubic phase structure with a lattice constant of $a = 1.011$ Å (JCPDS 71-2195). Both measurement results show that the stronger and sharper XRD phase peaks could be detected as the growth temperatures were increased. Therefore, the percentage of the crystalline phase of In_2O_3 nanostructures could get higher when the samples were grown at higher growth temperature, which was consistent with the SEM observations.

The normalized PL measurement results of the In_2O_3 nanostructures prepared by different growth conditions reveal the quality dependent characteristics as shown in Fig. 5. Since the bandgap energy of In_2O_3 is around 3.6 eV, we could exclude the origin of the PL as shown in Fig. 5 from the band-to-band transition. Namely, the transition could substantially be ascribed to the carrier recombination between the valence band and the oxygen vacancy-induced donor levels formed in the midst of the In_2O_3 bandgap [12]. However, the different crystallization quality of the In_2O_3 nanostructures could result in different transition path of carriers due to the different amounts of oxygen vacancies and defects generated during the growth [13]. The reason for electrical n-type property of In_2O_3 is that no enough oxygen atoms to catch electrons released from indium atom. The more electrons existing in crystal could fill up the oxygen vacancy-induced donor level and the Fermi energy will be raised up higher to be closer to the conduction band [14]. The Fermi energy levels filled up by different amount of electrons can be deemed as new energy states for optical transitions. A schematic diagram of relative states is shown in Fig. 6. E_1–E_3 represents main energy states between the conduction and the valence band caused by different amounts of electrons filled up the oxygen vacancy-induced donor levels. In our case, the worse quality sample grown at 500 °C would lead to a shorter wavelength emission and stronger emission intensity due to more oxygen vacancies and more electrons formed in the nanostructures which exhibited higher energy state E_1. With increasing growth temperature, the fewer electrons would produce due to better material quality and form lower energy states E_2 and E_3. Therefore, we could synthesize the In_2O_3 nanostructures emitting different wavelength peaks to span the whole blue–orange light region by adjusting these growth conditions. It is worth noting that the growth temperature could influence the

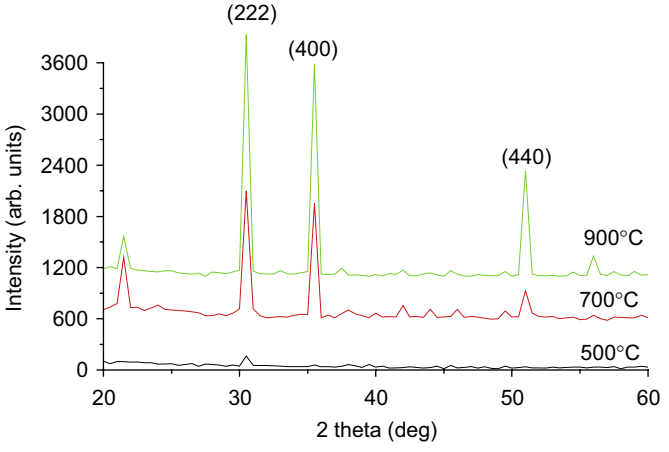

Fig. 4. XRD pattern of the In_2O_3 nanostructures grown at different growth temperatures.

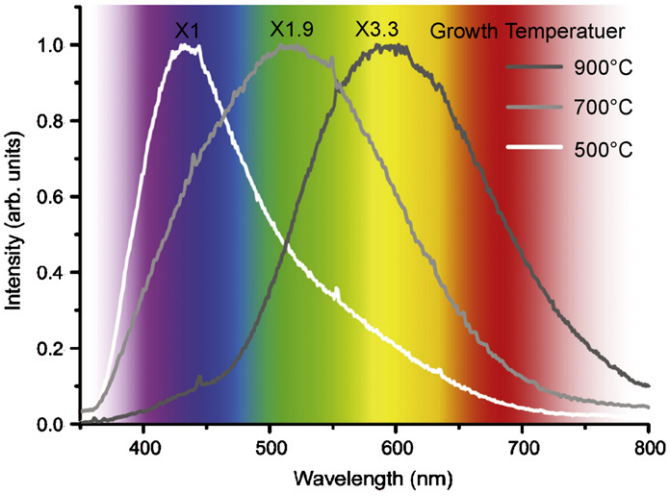

Fig. 5. Room temperature PL spectra of the In_2O_3 nanostructures grown at different growth temperatures.

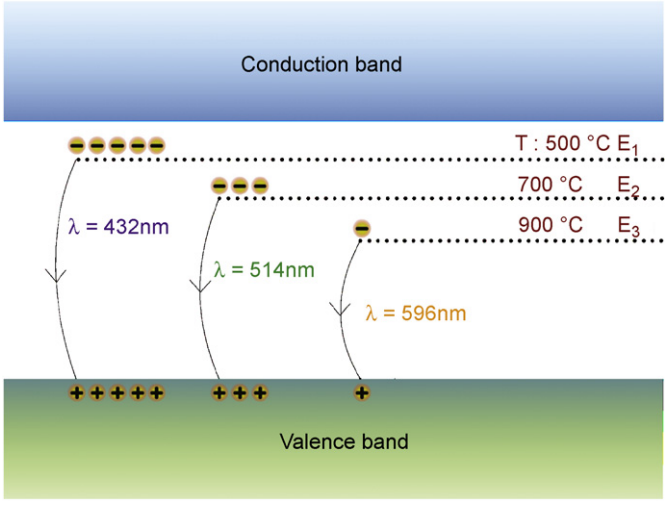

Fig. 6. Transition and emission mechanisms for In_2O_3 nanostructures.

optical transition energy in the nanostrcutures. Considering the oxygen vacancies, the vacancies could be repaired and would diminished in amount accordingly as we increased the growth temperature.

4. Conclusion

We have grown the In_2O_3 nanostructures at different growth temperatures by using the thermal evaporation method. The VLS process was dominant in the growth of the In_2O_3 nanostructures confirmed by the TEM images. Both SEM and XRD results revealed the clearer phase of In_2O_3 nanostructures as our samples were grown at higher growth temperature. The PL measurement results showed that In_2O_3 nanostructures could emit different broadband luminescence peaks ranging from 400 to 600 nm by adjusting growth temperature. Owing to the different amount of oxygen vacancies provided by different growth conditions, the optical transition energy of the In_2O_3 nanostructures becomes tunable, which could be beneficial for possible applications in white light illumination.

Acknowledgments

This work was supported by the MOE ATU program and in part by the National Science Council NSC 95-2120-M-009-008, NSC 96-2221-E009-092-MY3, NSC 96-2221-E009-093-MY3, and NSC 96-2221-E009-094-MY3, Republic of China.

References

[1] M. Emziane, R.L. Ny, Mater. Res. Bull. 35 (2000) 1849.
[2] I. Hamberg, C.G. Granqvist, J. Appl. Phys. 60 (1986) R123.
[3] C.G. Granqvist, Appl. Phys. A Mater. Sci. Process. 57 (1993) 19.
[4] M.S. Lee, W.C. Choi, E.K. Kim, C.K. Kim, S.K. Min, Thin Solid Films 279 (1996) 1.
[5] D.A. Magdas, A. Cremades, J. Piqueras, Appl. Phys. Lett. 88 (2006) 113107.
[6] C. Liang, G. Meng, Y. Lei, F. Phillipp, L. Zhang, Adv. Mater. 13 (2001) 1330.
[7] M.J. Zheng, L.D. Zhang, G.H. Li, X.Y. Zhang, X.F. Wang, Appl. Phys. Lett. 79 (2001) 839.
[8] Y. Li, Y. Bando, D. Golberg, Adv. Mater. 15 (2003) 581.
[9] C.H. Liang, G.W. Meng, Y. Lei, F. Phillip, L.D. Zhang, Adv. Mater. 13 (2001) 1330.
[10] C.H. Liang, L.C. Chen, J.S. Hwang, K.H. Chen, Y.T. Hung, Y.F. Chen, Appl. Phys. Lett. 81 (2002) 22.
[11] H.J. Chun, Y.S. Choi, S.Y. Bae, H.C. Choi, J. Park, Appl. Phys. Lett. 85 (2004) 461.
[12] H. Cao, X. Qiu, Y. Liang, Q. Zhu, M. Zhao, Appl. Phys. Lett. 83 (2003) 761.
[13] K.B. Sundaram, G.K. Bhagavat, Phys. Status Solidi 63 (1987) K15.
[14] C. Kittel, Introduction to Solid State Physics, Wiley, Hoboken, NJ, 2005.